CrystEngComm

ROYAL SOCIETY OF CHEMISTRY

PAPER

View Article Online
View Journal | View Issue

Cite this: *CrystEngComm*, 2025, **27**, 1619

Growth, anisotropy, and spectroscopy of Tm^{3+} and Yb^{3+} doped $MgWO_4$ crystals

Ghassen Zin Elabedine, [a] Rosa Maria Solé, [a] Sami Slimi,[a] Magdalena Aguiló,[a] Francesc Díaz,[a] Weidong Chen,[bc] Valentin Petrov[b] and Xavier Mateos †*[a]

Received 18th November 2024,
Accepted 3rd February 2025

DOI: 10.1039/d4ce01168f

rsc.li/crystengcomm

We report on an improved crystal growth process, reassessment of the orientation of the optical ellipsoid, and polarized spectroscopy of doped monoclinic magnesium monotungstate ($MgWO_4$) in a new dielectric frame. A set of crystals, including undoped, Yb^{3+}-doped, and Tm^{3+}-doped $MgWO_4$, were grown by the top-seeded solution growth (TSSG) method with $K_2W_2O_7$ as a solvent. This approach resulted in high-quality crystals with a significantly reduced growth time compared to those grown using Na_2WO_4. The crystal structures were confirmed by powder X-ray diffraction, and the lattice parameters were determined using Le Bail fitting. We review the growth methodology and emphasize the revision of the principal optical axes orientation in this biaxial crystal which differs substantially from previous reports. Polarized Raman spectroscopy was conducted based on this revised orientation. The absorption and stimulated emission cross-sections of the studied ions were derived for the principal light polarizations, comparing these findings with existing results to validate the new dielectric frame orientation.

1. Introduction

The divalent metal monotungstates, denoted as $M^{2+}WO_4$, find applications as scintillators[1] and, when doped with rare-earth ions (RE^{3+}), in solid-state lighting and lasers.[2–4] Historically the primary focus has been on their tetragonal scheelite-type phase, which occurs when M^{2+} = Ca^{2+}, Sr^{2+}, Ba^{2+}, or Pb^{2+}. Besides as laser hosts such crystals have proven to be highly suitable for Raman shifters. Their thermal conductivity (κ) is moderate, approximately 3 W m^{-1} K^{-1}.[5] In the tetragonal MWO_4 crystals, the RE^{3+} dopant ions replace the M^{2+} cations, however, the doping level is limited due to the mismatch of ionic radii and the need for charge compensation. Unfortunately, the tetragonal structure does not offer substantial transition cross-sections of the RE^{3+} ions for efficient lasing. Furthermore, the negative thermo-optic coefficients (dn/dt) for tetragonal $M^{2+}WO_4$ crystals typically cannot be offset by thermal expansion. Consequently, RE^{3+}-doped tetragonal $M^{2+}WO_4$ monotungstates garnered more attention for applications as phosphors, nano- and microcrystals.[6]

Besides the tetragonal scheelite structure family of divalent metal monotungstates, there has been a growing interest in recent years in laser applications of the monoclinic structure, which occurs for M^{2+} = Mg^{2+}, Zn^{2+}, Cd^{2+}, *etc.*[7] These compounds feature a crystal symmetry known as wolframite [(Fe,Mn)WO_4] type, which falls within the monoclinic class with the space group $P2/c$.[8] They exhibit a high degree of order with a single crystallographic site for the M^{2+} cations of six-fold oxygen coordination (site symmetry: C_2).[9] Two noteworthy representatives of this crystal family are magnesium monotungstate ($MgWO_4$), recognized as huanzalaite in its natural mineral state, and zinc monotungstate ($ZnWO_4$), alternatively named sanmartinite.

These crystals are optically biaxial, offering strong optical anisotropy. Due to their appealing optical and thermal properties, introducing RE^{3+} ions to enable laser operation has been under consideration. The crystal structure of the undoped $MgWO_4$ has been documented in ref. 10. As a host material, it is characterized by a relatively high thermal conductivity of κ ~8.7 W m^{-1} K^{-1},[11] as measured for a random crystal orientation. In recent years, significant efforts have been directed towards synthesizing nanocrystals and ceramics based on monoclinic $M^{2+}WO_4$ phases.[12–14] Initially, single-crystal $MgWO_4$ was explored as a scintillator.[14–16] Later, it was studied as a promising host for transition-metal ions such as Cr^{3+}, showing broad emission spectra in the near-infrared spectral range.[17] However, achieving laser operation with Cr^{3+}:$MgWO_4$ remains an ongoing challenge.

[a] *Física i Cristal·lografia de Materials (FiCMA), Universitat Rovira i Virgili (URV), 43007 Tarragona, Spain. E-mail: xavier.mateos@urv.cat*
[b] *Max Born Institute for Nonlinear Optics and Short Pulse Spectroscopy, Max-Born-Str. 2a, 12489 Berlin, Germany*
[c] *Fujian Institute of Research on the Structure of Matter, Chinese Academy of Sciences, Fuzhou, 350002 Fujian, China*
† Serra Húnter Fellow, Spain.

Previous research with RE^{3+} dopants primarily concentrated on the 1 μm spectral range by incorporating ytterbium (Yb^{3+})[3,18–20] and the 2 μm spectral range by incorporating thulium (Tm^{3+}).[21–26] Notably, a diode-pumped high-power laser based on Yb^{3+}:$MgWO_4$ was demonstrated,[20] delivering impressive 18.2 W near 1056 nm in a linearly polarized output with a slope efficiency of ~89%. Pulses as short as 125 fs at 1065 nm were obtained by semiconductor saturable absorber (SESAM) mode-locking (ML) of a Yb^{3+}:$MgWO_4$ laser at 117 Hz.[19] A continuous-wave (CW) diode-pumped Tm^{3+}:$MgWO_4$ laser generated an output power of 3.09 W in the 2022–2034 nm wavelength range with a slope efficiency of 50%.[20] Employing graphene for ML such a laser at a repetition rate of 76 MHz produced 86 fs pulses at 2017 nm with a bandwidth of 53 nm (ref. 21) while using single-walled carbon-nanotubes (SWCNTs), pulses as short as 76 fs could be generated at 2037 nm with a bandwidth of 64 nm for a repetition rate of 86.5 MHz.[25]

Previous studies have revealed various favorable spectroscopic characteristics of $MgWO_4$ crystals doped with RE^{3+} ions. These properties include significant anisotropy of the transition cross-sections for polarized light, relatively large Stark splitting of the ground states, and the presence of unevenly broadened spectral bands. These characteristics result from the low symmetry of the RE^{3+} site, where dopant ions replace the Mg^{2+} host-forming cations, and the significant difference in ionic radii between Mg^{2+} (0.72 Å)[27] and the RE^{3+} dopant (*e.g.*, the ionic radii of Tm^{3+} and Yb^{3+} for VI-fold coordination amount to 0.88 and 0.868 Å, respectively[27]), as well as the valence state difference between the dopant and host-forming cations, leading to distortion in the local crystal field. Charge compensation occurs by M^{2+} vacations or various valence impurity cations entering the interstitial positions.[28,29] Additionally, it was suggested that incorporation of monovalent alkali-metal cations (*e.g.*, Na^+ from the flux in the case of $MgWO_4$), play a crucial role in the modification of the spectroscopic properties of these crystals.[7,23]

Growing $MgWO_4$ crystals using the conventional Czochralski method is challenging due to their high-temperature phase transition. Instead, the top-seeded solution growth (TSSG) method is a well-documented and effective alternative for obtaining high-quality $MgWO_4$ crystals.[3,11] Early studies have shown that $MgWO_4$ crystals may exhibit notable defects affecting their optical properties.[3,30] These color centers and other defects may prevent the desired laser operation with Yb^{3+} and Tm^{3+} doped $MgWO_4$ crystals. Additionally, the growth duration of these crystals is a critical consideration (30 days of growth[3]). It can be improved by fine-tuning the growth parameters such as the choice of solvent (with lower viscosity, offering sufficient solubility of $MgWO_4$ and a wide enough crystallization region of monoclinic $MgWO_4$), solute/solvent ratio, seed orientation, cooling rate, and angular rotation velocity of the growing crystal.

In this work, high quality undoped $MgWO_4$ and Tm^{3+} and Yb^{3+} doped crystals were grown by the TSSG method with optimized growth time. For the first time to our knowledge, $K_2W_2O_7$ was used as a flux instead of Na_2WO_4. No additional post-growth annealing was applied. We provide a comprehensive analysis of the orientation of the optical indicatrix (dielectric frame) with respect to the crystallographic frame, measurements of the principal refractive indices and precise polarization-resolved spectroscopy. The present study revealed an unexpected deviation from the previously reported orientation of the optical ellipsoid used in earlier spectroscopic characterization of doped $MgWO_4$. The polarization-resolved spectroscopy of Tm^{3+} and Yb^{3+} doped $MgWO_4$ samples and the polarized Raman spectroscopy were performed according to the newly determined orientation of the principal optical axes.

2. Experimental

2.1 Crystal growth

Single crystals of $MgWO_4$ were grown using the TSSG method under similar conditions. The starting growth involved undoped $MgWO_4$ crystals, followed by two doped crystals with different RE^{3+} ion dopants, Tm^{3+} and Yb^{3+}.

All samples were grown in a vertical tubular furnace, using a Kanthal wire as the heating element and an Eurotherm 903P temperature controller/programmer connected to a thyristor. A type S thermocouple, located near the heater, was used to control the furnace temperature. For the undoped crystal, $K_2W_2O_7$ was used as a solvent with a molar ratio of the solution composition $K_2W_2O_7/MgWO_4$ = 75/25. The starting materials, K_2CO_3, K_2O, MgO and WO_3, were mixed in the appropriate ratios, weighting about 240 g, and placed in a platinum (Pt) crucible with a diameter of 40 mm and a height of 52 mm. The crucible was then positioned in the center of the furnace to maintain an axial temperature gradient of 1 °C cm^{-1}, ensuring that the bottom was hotter than the surface. The mixture was homogenized by maintaining the solution at 50 °C above the expected saturation temperature (T_{SA}) for 9 h. The T_{SA} was determined with a *b*-oriented $MgWO_4$ seed in contact with the solution surface. After accurately determining T_{SA} by monitoring the growth and dissolution of the seed, the growth process began with the same *b*-oriented $MgWO_4$ seed, while the solution temperature was gradually decreased by 40 °C at a rate of 0.12 °C h^{-1}. The crystal was rotated at 60 rpm. Subsequently, it was removed from the solution and cooled slowly to room temperature (RT) at a rate of 40 °C h^{-1}. The obtained crystals were transparent and free from defects, with typical dimensions of 11.3 × 10.6 × 14.9 mm^3 along the $a^* \times b \times c$ directions, see Fig. 1(a). Several identical crystal growth attempts were carried out, resulting in crystals with very similar dimensions and quality.

For the doped crystals, a Pt crucible with a length of 47 mm and a diameter of 45 mm was used due to availability. The same starting materials were mixed. For the Tm-doped

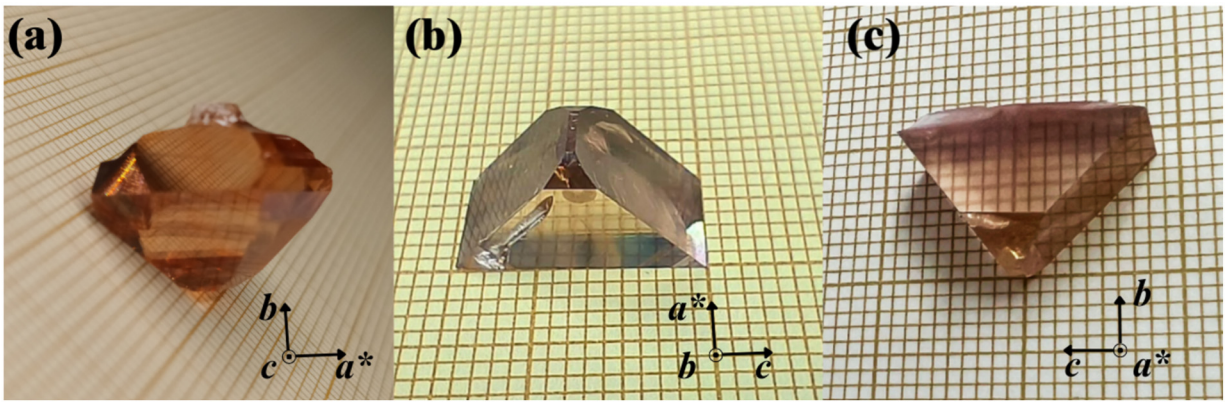

Fig. 1 Photographs of the crystals grown along the [010] direction: (a) undoped $MgWO_4$, (b) Tm^{3+}:$MgWO_4$, and (c) Yb^{3+}:$MgWO_4$.

crystal, Tm_2O_3 was added according to the formula $Tm_{0.1}$-$Mg_{0.9}WO_4$, with the mixture weighting 150 g. A growth approach similar to that used for the undoped crystal was applied, including growth direction, rotation speed, cooling rate, thermal gradient, and speed. The dimensions of the obtained crystals were 9.1 × 14.8 × 10.3 mm^3 (a^* × b × c). The as-grown crystals were transparent, as shown in Fig. 1(b). Similarly, the Yb-doped crystals were grown by adding Yb_2O_3 to the starting material, assuring a starting concentration of 10 at% of Yb^{3+} relative to Mg^{2+} in the solution. The 10% dopant concentration in the solution was chosen to reproduce the crystals reported in the literature.[3,24] The resulting crystals typically measured 6.1 × 7.7 × 12.9 mm^3 (a^* × b × c). These crystals were transparent, free of cracks and inclusions as shown in Fig. 1(c). All the crystals exhibited a wine-brown coloration. We attribute the coloration in our crystals to the presence of oxygen vacancies. In order to remove them, we have treated the crystals thermally in air, under some conditions of temperature and time. Because of the large volume of the crystals, the oxygen did not penetrate significantly to remove those vacancies. For that reason, after the thermal treatment we still observe the coloration.

Growing the crystals took less than 15 days each, which is twice as fast compared to previously reported growth rates for the Yb-doped $MgWO_4$ crystals, amounting to 30 days to achieve similar dimensions.[3] This improved growth rate is attributed to the use of $K_2W_2O_7$ as the solvent, which facilitates faster mass and heat transport for nucleation and growth due to the lower viscosity of the solution, resulting from the higher WO_3 content.

Microprobe analysis using wavelength dispersive spectroscopy, conducted with a Cameca Camebax SX-100 analyzer, determined the actual doping levels in the crystals. The Tm^{3+} doping level was found to be 0.78 at% (ion density: N_{Tm} = 1.2 × 10^{20} cm^{-3}), resulting in a segregation coefficient $K_{Tm} = C_{crystal}/C_{solution}$ of 0.078. For the Yb^{3+} ion, the doping level was determined to be 1.11 at% (ion density: N_{Yb} = 1.69 × 10^{20} cm^{-3}) with a segregation coefficient K_{Yb} of 0.111.

2.2 Characterization methods

To study the changes in unit cell parameters due to Yb^{3+} and Tm^{3+} doping and to calculate the linear thermal expansion tensor, small $MgWO_4$ single crystals were grown on a Pt rod immersed in the solution. After the crystals were cleaned, they were ground in an agate mortar and pestle for X-ray diffraction (XRD) measurements.

The unit cell parameters of the three crystals were determined from powder XRD analysis using a Bruker-AXS D8 Advance diffractometer equipped with a vertical θ–θ goniometer and Cu Kα radiation. Diffracted X-ray were detected using a LynxEye-XE-T position-sensitive detector (PSD) featuring an opening angle of 2.94°. Data were acquired over the 2θ range of 10° to 80°, with a step size of 0.02° and a step time of 2 s. The obtained XRD patterns were analyzed using Le Bail fitting, facilitated through Topas V6 software. The initial model for the Le Bail fitting was based on the crystal structure of undoped $MgWO_4$ (Powder Diffraction File™ (PDF®), PDF card #73-0562, The International Centre for Diffraction Data (ICDD®), ICSD code 22357).

To determine the linear thermal expansion tensor of $MgWO_4$, powder XRD measurements were conducted at temperatures ranging from 30 to 600 °C. The heating rate was 10 °C min^{-1}, with a delay time of 300 s before each measurement. The powder sample was placed inside an MCT-HIGHTEMP chamber with a Pt heating element. Data were collected for the same settings except for the step time which was 1 s.

In order to compare the crystalline quality when doping, a $2\theta/\omega$ scan of the (030) reflection (rocking curve) of the $MgWO_4$ and Yb:$MgWO_4$ single crystals was recorded with the same X-ray equipment used for the previous measurements. The rocking curves were obtained by scanning within a range of ±1.2° ω width by taking 120 frames at a step size of 0.02° and 10 s per frame.

The refractive indices were systematically determined for polarization along the three principal optical axes for each crystal investigated using a prism-film coupler, specifically a

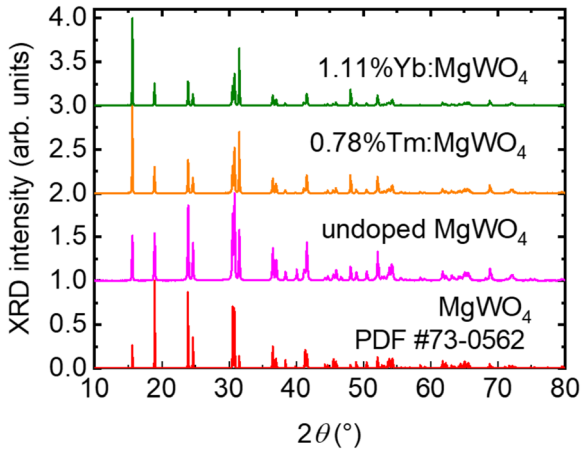

Fig. 2 Measured powder X-ray diffraction (XRD) results for the Tm-doped, Yb-doped, and undoped $MgWO_4$, and theoretical pattern for undoped $MgWO_4$ based on PDF card #73-0562.

Metricon 2010 instrument. The samples used were 2 mm thick in the *b* direction, enabling the measurement of the refractive index for the three principal polarizations.

A Varian CARY 5000 spectrophotometer equipped with a Glan–Taylor polarizer was used to measure the polarized absorption spectra of cubic samples oriented in the dielectric frame for the $^3H_6 \rightarrow {}^3H_4$ Tm^{3+} electronic transition and the $^2F_{7/2} \rightarrow {}^2F_{5/2}$ Yb^{3+} electronic transition.

Luminescence measurements were performed by exciting the same samples with a laser diode emitting at 966 nm for Yb^{3+} and 793 nm for Tm^{3+}. The emitted light was collected in a 90° configuration. A Glan–Taylor polarizer was employed to discriminate the polarization of the luminescence.

The decay time of the luminescence was quantified using an optical spectrum analyzer (OSA, Yokogawa, model AQ6375B) in conjunction with a 2 GHz digital oscilloscope (Tektronix DPO5204B). The excitation was performed at very low power and directed towards the edge of the sample to mitigate reabsorption effects.

The Raman spectra were acquired using polarized light in conjunction with a Renishaw Via Raman confocal microscope equipped with a 50× objective. The excitation wavelength used was 633 nm, generated by a He–Ne laser, and the spectral resolution was approximately 1 cm^{-1}.

3. Results and discussion

3.1 Phase structure and lattice parameters

The crystal structure and phase were confirmed through XRD analysis. The RT XRD patterns for the 0.78% Tm:$MgWO_4$, 1.11% Yb:$MgWO_4$ and undoped $MgWO_4$ are presented in Fig. 2. The diffraction peaks exhibited by the crystals grown in this work, in terms of both relative intensity and position, closely align with those outlined in the crystallographic database for undoped $MgWO_4$, see Fig. 2. The crystal structure of $MgWO_4$ is monoclinic (centrosymmetric point group 2/*m*, space group – *P*2/*c*, No. 13). It is important to emphasize that for the crystallographic frame we adopt the $a < c$ setting with *b* corresponding to the monoclinic axis according to the *P*2/*c* space group, and in addition the convention of $\beta > 90°$ for the monoclinic angle[8,10] as well as righthandedness of the frame for univocal correspondence with other reference frames.

In the pursuit of comprehending the structural modifications, the unit cell parameters of the three crystals were determined using the Le Bail method, Fig. 3.[31] Initial unit cell parameters for the Le Bail refinement were extracted from.[32] As anticipated, the obtained unit cell parameters and volume in Table 1 were larger for the doped crystals due to the larger ionic radii of the doping ions compared to Mg^{2+}.[27]

The analysis of the rocking curves of the (030) reflection of $MgWO_4$ and Yb:$MgWO_4$ single crystals consists of two peaks for each crystal, corresponding to the $K_{\alpha1}$ and $K_{\alpha2}$ radiation from the X-ray source. For the evaluation of the crystals, we fitted both peaks to pseudo-Voigt functions. We have focused on $K_{\alpha1}$ to extract conclusions from the measurements because of its higher intensity and found a full width at half maximum (FWHM) of the reflection to be 0.036° for $MgWO_4$ and 0.031° for Yb:$MgWO_4$, indicating the absence of significant difference between them and, due to the very small values, the high crystals quality.

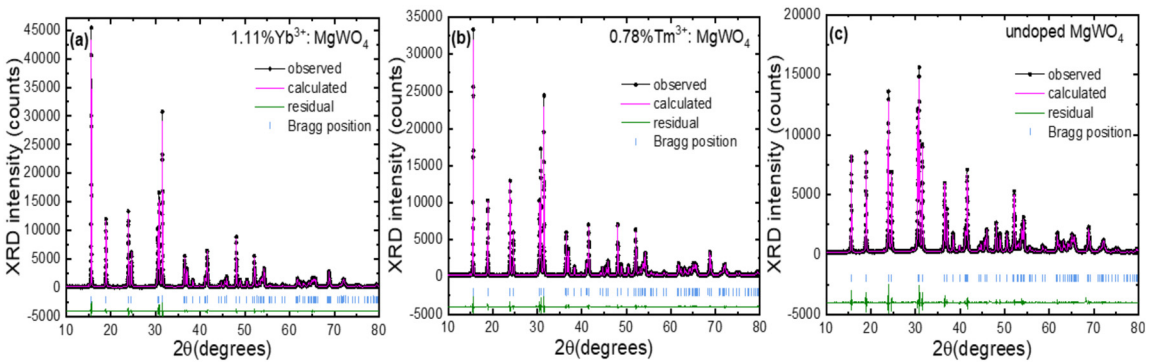

Fig. 3 Le Bail refinement of (a) Yb doped $MgWO_4$ (b) Tm doped $MgWO_4$ (c) undoped $MgWO_4$ crystals: experimental (black), calculated (magenta) and differential (green), vertical dashes mark the Bragg reflections.

Table 1 The unit cell parameters using Le Bail refinement

Crystal	a (Å)	b (Å)	c (Å)	β (°)	Volume (Å^3)
$MgWO_4$	4.686(7)	5.674(1)	4.927(8)	90.710(7)	131.036(5)
0.78%Tm:$MgWO_4$	4.693(1)	5.677(1)	4.931(6)	90.741(6)	131.382(9)
1.11%Yb:$MgWO_4$	4.695(1)	5.677(9)	4.932(7)	90.753(7)	131.492(3)

3.2 Linear thermal expansion tensor

The thermal expansion of undoped $MgWO_4$ was studied by recording XRD patterns at temperatures of 30, 50, 100, 200, 300, 400, 500 and 600 °C. The unit cell parameters (a, b, c, and β) were determined for each temperature using the Le Bail method. All lattice constants increased linearly with temperature (see Fig. 4). The volume of the unit cell (V) showed the same behaviour of increasing with temperature.

The coefficients of the linear thermal expansion tensor of $MgWO_4$ in the crystallophysic frame were obtained from the slope of the linear fits of the thermal evolution of the normalized unit cell parameters of this phase (see Fig. 5). This tensor is presented below:

$$(a'_{ij}) = \begin{pmatrix} 11.74 & 0 & 4.82 \\ 0 & 8.26 & 0 \\ 4.82 & 0 & 8.59 \end{pmatrix} \times 10^{-6}\ \mathrm{K}^{-1}$$

with X'_1 parallel to a axis, X'_2 parallel to b axis and X'_3 parallel to c^* direction ($c^* = a \times b$), defining an orthogonal auxiliary frame.

By diagonalizing the previous tensor, the linear thermal expansion tensor of $MgWO_4$ in the eigenframe is obtained:

$$(a_{ij}) = \begin{pmatrix} 15.24 & 0 & 0 \\ 0 & 8.26 & 0 \\ 0 & 0 & 5.09 \end{pmatrix} \times 10^{-6}\ \mathrm{K}^{-1}$$

with the principal axis X_1 located at 35.9° (counterclockwise) from the a axis, X_2 parallel to the b axis, and X_3 at 36.6° (counterclockwise) from the c axis when the b axis shows towards the observer. The thermal expansion ellipsoid is depicted in Fig. 6.

The above values can be compared with our previous results obtained for Ho:$MgWO_4$:[7] the corresponding principal values were very close, 14.8, 8.09, and 5.07 × 10^{-6} K^{-1}, respectively, and the rotation angle for the X_1 axis was 37.35° for a monoclinic angle of β = 90.74°. This good agreement shades more doubt in the accuracy of the thermal expansion results reported in ref. 11 for Cr^{3+}:$MgWO_4$ using a dilatometer.

3.3 Orientation of the optical indicatrix

The monoclinic $MgWO_4$ crystal is optically biaxial and as such possesses three principal optical directions (axes of the optical indicatrix) forming an orthogonal frame, which are known as N_g, N_m and N_p, according to the notation of the corresponding refractive indexes $n_g > n_m > n_p$, where the

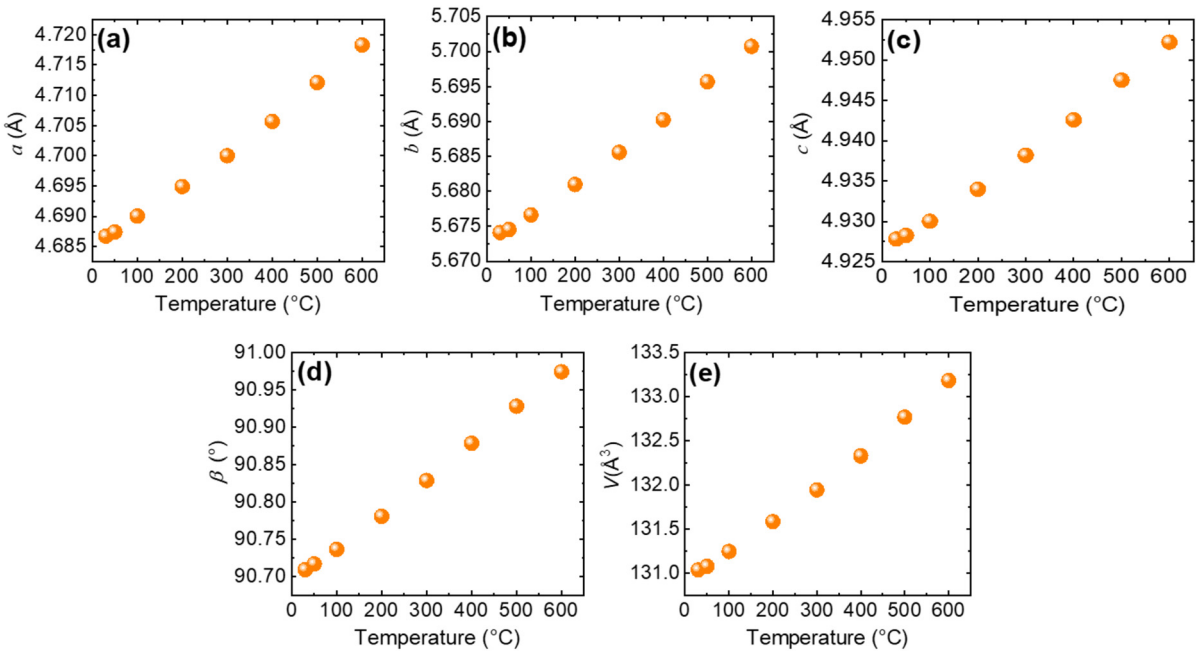

Fig. 4 (a–e) Linear dependence of lattice constants a, b, c, and β, and the volume of the unit-cell V of undoped $MgWO_4$ crystal on temperature.

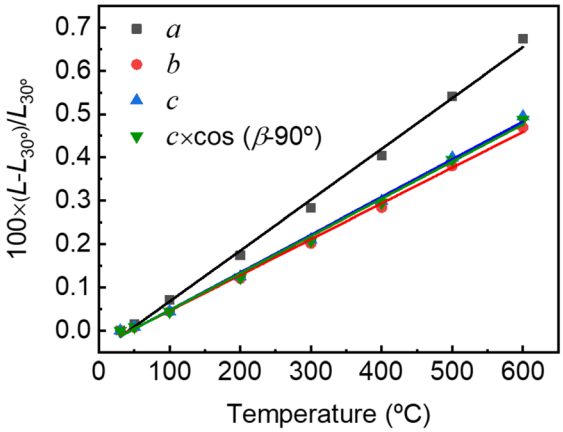

Fig. 5 Normalized unit cell parameters of $MgWO_4$ *versus* temperature, (L = *a*, *b*, *c*, and *c* × cos(β − 90°)).

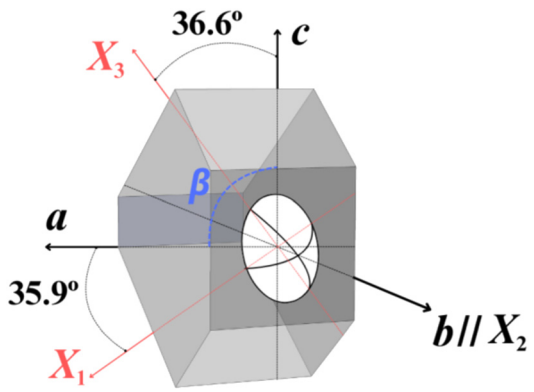

Fig. 6 Thermal expansion ellipsoid of $MgWO_4$.

subscript *g* denotes the highest refractive index, and *p* denotes the lowest one. One of the principal optical axes (in this case N_m) aligns with the C_2 symmetry axis (the *b* axis), while the other two axes (N_p and N_g) lie in the orthogonal mirror plane (the *a*–*c* plane). These principal axes define the principal planes and light polarized in or perpendicular to these planes does not experience polarization rotation upon propagation.

Initially, the orientation of the principal optical axes for 1.25 at% Yb:$MgWO_4$ was studied using transmission measurements with a polarizing microscope without information on the refractive index, hence they were denoted in a neutral manner, *e.g.* as *XYZ*.[3] In this work, the rotation of the two principal optical axes lying in the *a*–*c* plane around the *b*-axis of the quasi-orthogonal *abc* frame was measured to be in the 36.4–37.1° range with an obvious error seen comparing with the monoclinic angle β given (see Fig. 2 in ref. 3). This error was rectified in ref. 23 in terms of rotation of the dielectric frame relative to the *abc* frame in the opposite direction with the two angles in the *a*–*c* plane being the same. The refractive indices were estimated then in this new frame from transmission measurements near 1.2 μm: n_p = 1.97, n_m = 2.03, and n_g = 2.13 with an error of ± 0.02 which enabled the assignment of N_g, N_m and N_p.

Apart from the above controversial assignment of the orthogonal dielectric frame $N_pN_mN_g$, notable disparities surfaced between the respective spectroscopic studies, encompassing variations not only in the absolute values of absorption and stimulated emission (SE) cross-sections for the three polarizations but also in the spectral shape, with similarities observed in absorption cross-sections and marked dissimilarity in SE cross-sections.[3,20,23,24] The uncertainties led to the study and presentation of the Ho- and Er-doped $MgWO_4$ spectroscopy in the crystallographic frame *abc*.[7,30] For laser applications, however, spectroscopy in the orthogonal dielectric frame is desirable, because although this does not guarantee that cross-sections are maximized, more important is to ensure that polarization–rotation (waveplate) effects are absent in a laser emitting polarized radiation. The above discrepancies raised concerns, prompting a reassessment of the orientation of our doped $MgWO_4$ crystals. Initial attempts using the dielectric frame orientation from[23] yielded inaccurate results for our samples, Tm:$MgWO_4$ and Yb:$MgWO_4$, further justifying a thorough investigation into the relative frame orientation.

Subsequent to orienting our samples in the crystallographic *abc* frame through XRD, an examination of the principal optical axes was conducted using a crossed polarizers setup. The 2 mm thick samples, precisely cut perpendicular to the *b* direction, were positioned between two crossed Glan–Taylor polarizers. Through systematic rotation (with a goniometer with a precision of better than 1°), we successfully identified the principal optical axes in the *a*–*c* plane. Remarkably, one principal optical axis deviated by 6 ± 1° from the *c* direction (easily detectable as a natural edge of the grown crystal and confirmed by XRD), while the other was found to be exactly at 90° from the first zero transmission position. This consistent observation was replicated across all examined samples. The substantial deviation from the previously reported positions of these axes[3,23] solidified our suspicions, creating the need for an additional confirmation.

To substantiate our findings, the next investigative step involved determining the refractive index at various angles using the same goniometer relative to the *c* crystallographic axis for our undoped $MgWO_4$. The refractive index was measured with the prism coupler instrument using linearly polarized light at 633 nm and rotating the 2 mm thick polished plate around the *b*-axis. As shown in Fig. 7, knowing that N_g aligns with the highest refractive index while N_p corresponds to the lowest refractive index, our measurements corroborated that N_g is located at 5° from the *c* direction when rotating the crystal clockwise, as depicted in Fig. 7(a) and (b). Importantly, these refractive index measurements align closely with the results obtained through the crossed polarizers setup, providing further confirmation for the revised orientation of the dielectric frame of our crystal.

Based on the reproducible results obtained with different samples, we confidently assert that the dielectric frame

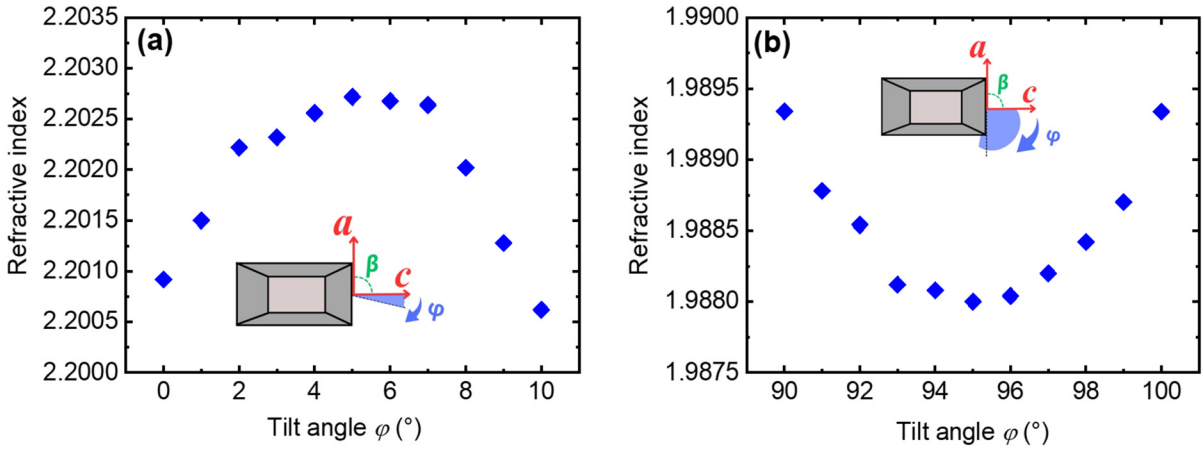

Fig. 7 Refractive index of $MgWO_4$ crystal at 633 nm for different angles φ of the polarization relative to the c crystallographic axis: (a) for the N_g principal optical direction, and (b) for the N_p principal optical direction. Inset – rotation direction of the crystal.

orientations reported in earlier studies on $MgWO_4$-based crystals were inaccurate. Our proposed orientation, supported by a comprehensive study, diverges from previous reports. Earlier assertions placed N_g at 36.4° from the a direction,[3,23] whereas our findings conclusively determine that N_g is located at 5 ± 1° from the c direction as shown in Fig. 8. Similarly, N_p was previously reported at 37.1° from the a direction, but our results definitively place N_p at 6 ± 1° from it. Thus, the previously reported substantial angles for $MgWO_4$ between the crystallographic and optical axes are likely inaccurate. Fig. 8 illustrates the correct orientation we propose for the monoclinic $MgWO_4$ crystal.

Since laser elements are cut for propagation within one of the principal planes in order to avoid waveplate like polarization rotation effects, it is of practical interest to calculate the thermal expansion along the three dielectric axes of the newly determined frame. Matrix transformation gives $\alpha_p = 12.71 \times 10^{-6}\ K^{-1}$, $\alpha_m = 8.26 \times 10^{-6}\ K^{-1}$, and $\alpha_g = 7.62 \times 10^{-6}\ K^{-1}$.

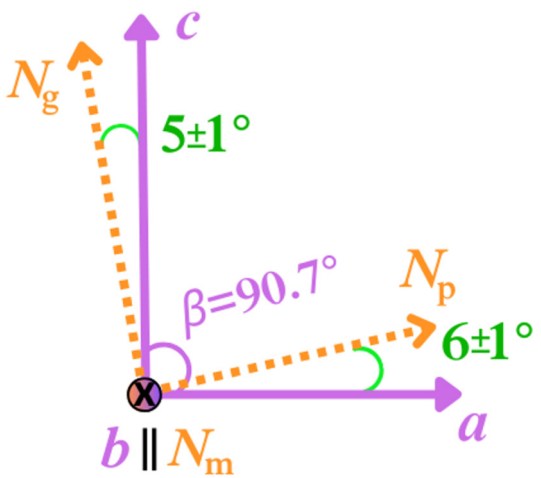

Fig. 8 Orientation of the optical indicatrix axes (N_p, N_m, N_g) forming the orthogonal dielectric frame with respect to the crystallographic frame (a, b, c) in monoclinic $MgWO_4$.

3.4 Refractive index measurements

The refractive indices of the three different samples were measured with the prism coupler device at various angles relative to the crystallographic axes to confirm the consistency of the angle between the principal optical and crystallographic axes.

As previously mentioned, using a 633 nm He–Ne laser, we verified that the N_g axis, which is associated with the highest refractive index, is located at an angle of 5 ± 1° from the c direction. Similarly, the N_p axis, with the lowest refractive index, is situated at an angle of 95 ± 1° from the c direction, while the N_m axis is aligned parallel to the b direction. Table 2 presents the refractive indices along the three principal optical axes for the grown crystals at 633 nm.

3.5 Polarized Raman spectroscopy

Polarized Raman spectra of $MgWO_4$ were previously presented in ref. 23 for Tm doping and in ref. 20 for Yb doping. To further characterize the doped crystals in the newly determined dielectric frame, we measured the polarized Raman spectra for both Tm^{3+}:$MgWO_4$ and Yb^{3+}:$MgWO_4$ at RT, as illustrated in Fig. 9. We used Porto's notation $m(nk)\bar{l}$, where 'm' and '$\bar{l}$' indicate the propagation directions of the excitation and scattered light, respectively, while 'n' and 'k' represent the corresponding polarization states.

Table 2 Refractive index for light polarization along N_p, N_m, and N_g for the undoped, Tm^{3+} doped, and Yb^{3+} doped $MgWO_4$ at 633 nm

Crystal	n_p	n_m	n_g
$MgWO_4$	1.9880	2.0478	2.2027
Tm:$MgWO_4$	1.9889	2.0478	2.2002
Yb:$MgWO_4$	1.9894	2.0476	2.2011

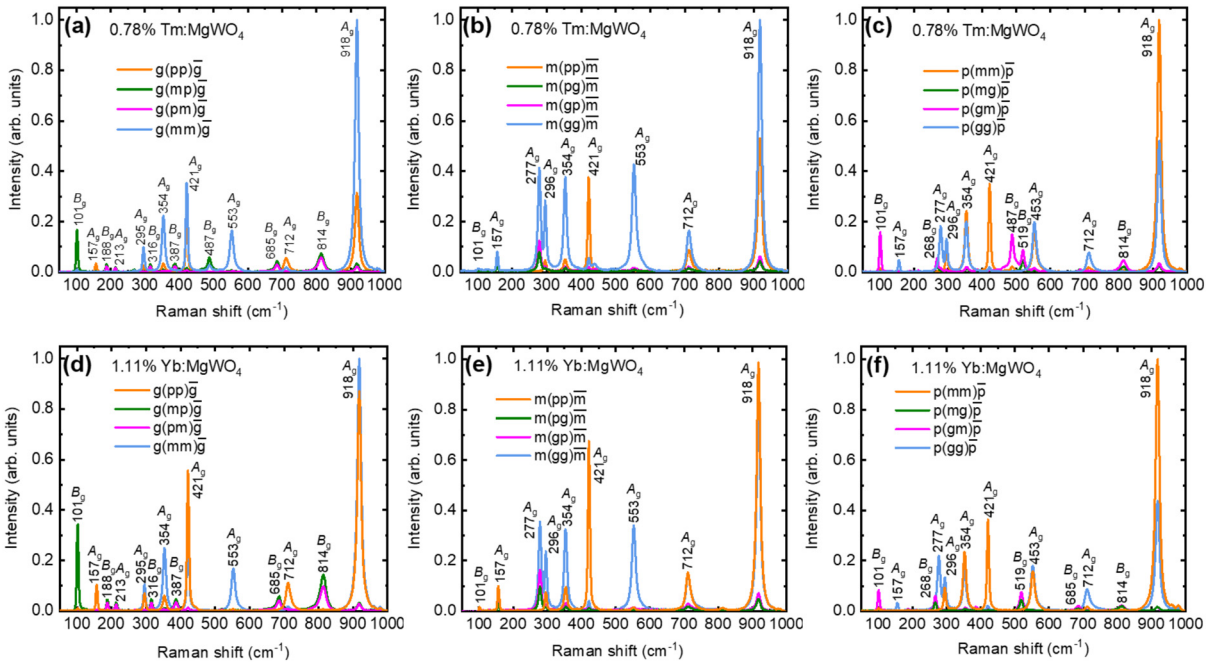

Fig. 9 Polarized Raman spectra for $g(\_)\bar{g}$, $m(\_)\bar{m}$, and $p(\_)\bar{p}$ of (a–c) Tm doped $MgWO_4$ crystal and (d–f) Yb doped $MgWO_4$ crystal. The excitation wavelength was 633 nm.

In the monoclinic structure of $MgWO_4$, there are two unit formulas per unit cell ($Z = 2$). According to factor group theory, 36 lattice modes are predicted at the centre of the Brillouin zone: $\Gamma(k = 0) = 8A_g + 10B_g + 8A_u + 10B_u$. Of these, 18 modes are Raman-active (even modes A_g and B_g), and 18 are IR-active (odd modes A_u and B_u). All the modes for $MgWO_4$ were assigned in ref. 33.

In the Tm^{3+}:$MgWO_4$ and Yb^{3+}:$MgWO_4$ crystals, the most intense mode, occurring around 918 cm^{-1}, corresponds to symmetric stretching W–O vibrations (v_1 mode, A_{1g} symmetry) within the WO_6 octahedra, while modes around 813 cm^{-1} and 711 cm^{-1} are assigned to asymmetric stretching (v_2 mode, E_g symmetry). Notably, a trend in peak intensities is evident. For instance, the peak at approximately 918 cm^{-1} (an A_g mode) is prominent in the *pp*, *mm*, and *gg* polarizations for different directions of excitation and scattered light, while it is less pronounced in other polarizations. This pattern is observed for several A_g mode peaks. Conversely, B_g modes, such as those around 813 cm^{-1} and 102 cm^{-1}, are less pronounced in the *pp*, *mm*, and *gg* polarizations and clearer in other polarizations.

When comparing our Raman spectra of Yb:$MgWO_4$ crystal with those reported in ref. 20 for $m(\_)\bar{m}$ configuration, notable differences in peak intensities are observed, particularly for the $m(pg)\bar{m}$ polarization configuration. In this work, $m(pg)\bar{m}$ shows unexpectedly high intensities across several A_g modes, comparable to $m(pp)\bar{m}$, while in the present measurements, $m(pg)\bar{m}$ yields much lower

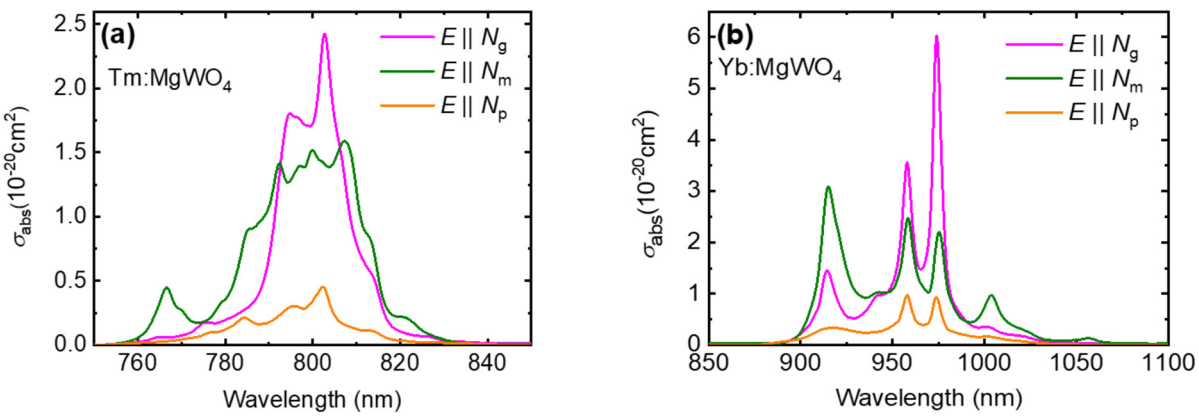

Fig. 10 Absorption cross-sections, σ_{abs}, for light polarizations $E||N_g$, N_m, and N_p for: (a) Tm^{3+} doped $MgWO_4$ crystal and (b) Yb^{3+} doped $MgWO_4$ crystal.

intensities. This discrepancy may indicate possible differences in crystal orientation but one cannot rule out the effect of different actual doping levels as well.

3.6 Optical spectroscopy

Polarized optical absorption measurements of Tm^{3+}:$MgWO_4$ and Yb^{3+}:$MgWO_4$ at RT were performed in the newly determined dielectric frame. Fig. 10 depicts the obtained absorption cross-sections (σ_{abs}) for the Tm^{3+} and Yb^{3+} doped $MgWO_4$ crystals, derived as $\sigma_{abs} = \alpha_{abs}/N_{Tm/Yb}$, where α_{abs} is the measured absorption coefficient, and N_{Tm} and N_{Yb} are the actual Tm^{3+} and Yb^{3+} ion density respectively. The polished cubic samples had dimensions of 4.74 × 6.04 × 5.34 mm^3 for Tm:$MgWO_4$ and 2.86 × 3.57 × 2.56 mm^3 for Yb:$MgWO_4$, both aligned along the principal optical directions N_p, N_m, and N_g, respectively.

High-brightness Ti–sapphire lasers or high-power AlGaAs diode lasers, emitting at approximately 800 nm, are suitable for pumping Tm^{3+}-doped crystals due to the $^3H_6 \rightarrow {}^3H_4$ transition of the Tm^{3+} ion. The maximum absorption cross-section (σ_{abs}) of Tm^{3+}:$MgWO_4$ amounts to 2.42 × 10^{-20} cm^2 at 803 nm, for light polarization $E||N_g$, and the corresponding absorption bandwidth (FWHM) is 15.5 nm, see Fig. 10(a). The σ_{abs} values are lower for the other principal polarizations. For $E||N_p$, σ_{abs} = 0.45 × 10^{-20} cm^2 at 802 nm, and for $E||N_m$, σ_{abs} = 1.59 × 10^{-20} cm^2 at 807 nm. Notably for $E||N_m$, the absorption bandwidth is superior, FWHM = 20 nm. The absorption bands around 800 nm are in general significantly wider than what is typically observed in monoclinic double tungstates such as Tm^{3+}:$KLu(WO_4)_2$. In the latter, for $E||N_m$ the absorption cross-section (σ_{abs}) reaches a value of 5.95 × 10^{-20} cm^2 at 802 nm, yet the absorption bandwidth is 4 nm.[34] Such broadband absorption behavior significantly simplifies the task of wavelength stabilization for AlGaAs pump laser diodes.

Fig. 10(b) shows the polarized absorption cross-section of Yb^{3+}:$MgWO_4$ around 1 μm, associated with the $^2F_{7/2} \rightarrow {}^2F_{5/2}$ electronic transition. Yb^{3+}:$MgWO_4$ features strongly anisotropic absorption properties. The maximum σ_{abs} amounts to 6.1 × 10^{-20} cm^2 at 974 nm, corresponding to a FWHM of 6 nm, for light polarization $E||N_g$, and this peak is associated with the so-called zero-phonon-line (ZPL) in absorption for the Yb^{3+} ion. When compared to Yb:$KLu(WO_4)_2$ with its σ_{abs} = 1.47 × 10^{-19} cm^2 at 981.1 nm ($E||N_m$), the absorption in Yb^{3+}:$MgWO_4$ is roughly two times lower but has a broader FWHM (6 *vs.* 3.5 nm).[32] For the other two polarizations, the absorption at this wavelength is lower: σ_{abs} = 2.24 × 10^{-20} cm^2 for $E||N_m$, and σ_{abs} = 0.94 × 10^{-20} cm^2 for $E||N_p$. Notably, these maximum σ_{abs} values are almost twice as high as those reported for the isostructural Yb^{3+}:$ZnWO_4$, for which a maximum σ_{abs} of 2.73 × 10^{-20} cm^2 at 973.5 nm was measured with a FWHM = 6 nm, for $E||N_g$.[35]

In the case of Tm-doping, the results obtained in the *XYZ* frame[22,24] are very close to our present results. Comparing with previously published absorption spectra, the difference is stronger for Yb-doping: the cross-sections obtained in ref. 3 in the *XYZ* frame are much lower although the spectral shapes look similar. The results in ref. 20 are very close to the present ones since they were obtained after an independent alignment in the dielectric frame $N_pN_mN_g$ between crossed polarizers and were thus independent of the exact frame location relative to the crystallographic frame.

The SE cross-section, σ_{SE}, was calculated using a combination of two methods. The first method employed the Füchtbauer–Ladenburg (F–L) equation[36] based on the measured luminescence intensity $W(\lambda)$:

$$\sigma^i_{SE}(\lambda) = \frac{\lambda^5}{8\pi\langle n\rangle^2 \tau_{rad} c} \frac{W_i(\lambda)}{1/3 \sum\limits_{j=p,m,g} \int \lambda' W_j(\lambda') \mathrm{d}\lambda'}$$

where λ denotes the luminescence wavelength, $\langle n\rangle$ is the refractive index at the average emission wavelength; τ_{rad} is the radiative lifetime associated with the $^3F_4$ state of Tm^{3+} and the $^2F_{5/2}$ state of Yb^{3+}, c is the speed of light; and the subscripts i and $j = p, m, g$ indicate the polarization state.

The second approach used was based on the reciprocity method (RM),[37] using the Stark splitting data determined in ref. 23 for the Tm^{3+} ion and in ref. 20 for the Yb^{3+} ion:

$$\sigma^i_{SE}(\lambda) = \sigma^i_{abs}(\lambda) \frac{Z_1}{Z_2} \exp\left(-\frac{hc/\lambda - E_{ZPL}}{kT}\right),$$

where σ^i_{abs} is the absorption cross-section for the i-th polarization, h is Planck's constant, k is the Boltzmann constant, T is the crystal temperature (RT), E_{ZPL} is the energy difference between the lowest Stark sub-levels of the two multiplets involved in the transition (ZPL), and Z_l are the partition functions of the lower (l = 1) and upper (l = 2) manifolds.

The maximum SE cross-section (σ_{SE}) for Tm^{3+}:$MgWO_4$ is observed at 1876 nm for $E||N_m$, amounting to 3.33 × 10^{-20} cm^2, see Fig. 11(a). For Yb^{3+}:$MgWO_4$, the maximum σ_{SE} reaches 6.63 × 10^{-20} cm^2 at 1058 nm, again for $E||N_m$, while for $E||N_g$ and $E||N_p$, σ_{SE} at the same wavelength drops to 1.98 × 10^{-20} and 0.54 × 10^{-20} cm^2, respectively. Notably, for $E||N_g$, maximum σ_{SE} occurs at 974 nm, reaching 5.93 × 10^{-20} cm^2, which is close to the maximum value observed for $E||N_m$, see Fig. 11(b). For both dopant ions, a strong anisotropy of the SE cross-section is observed, implying a natural selection of a linear polarization for laser emission.

The obtained SE cross-sections for Tm^{3+}:$MgWO_4$, are higher for the two dominating polarizations ($E||N_g$ and $E||N_m$) than the previously obtained values in what was thought to be the dielectric frame, both when denoted as *XYZ*[24] and as $N_pN_mN_g$.[23] For Yb^{3+}:$MgWO_4$, the difference compared to the *XYZ* assumption[3] is much larger, showing in roughly two times higher values and very different shapes, whereas minor discrepancies are observed comparing with results reported in ref. 20 in the $N_pN_mN_g$ frame.

For quasi-3-level laser systems the expected oscillation wavelength can be estimated from the corresponding gain

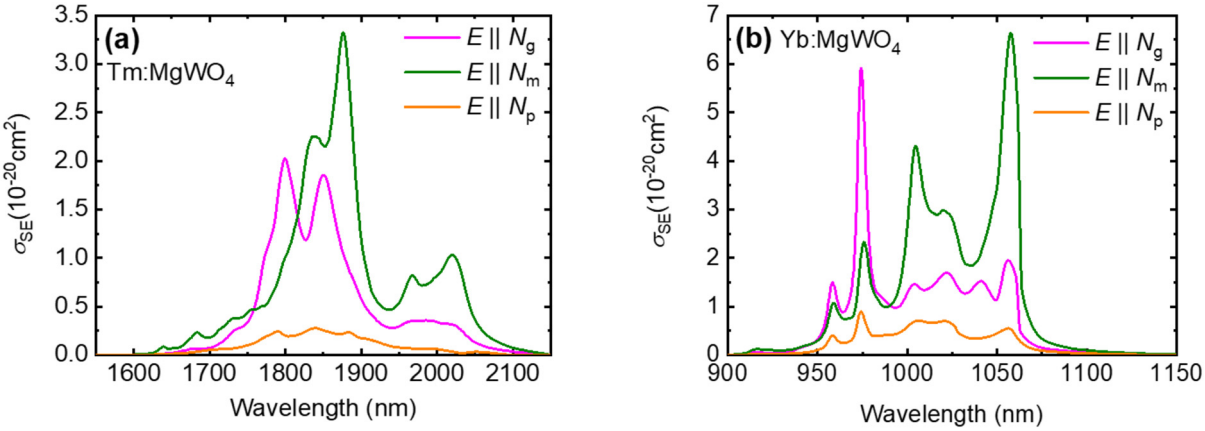

Fig. 11 Stimulated emission cross-sections, σ_{SE}, for the principal light polarizations $E||N_p$, N_m, and N_g of (a) Tm^{3+} doped $MgWO_4$ crystal and (b) Yb^{3+} doped $MgWO_4$ crystal.

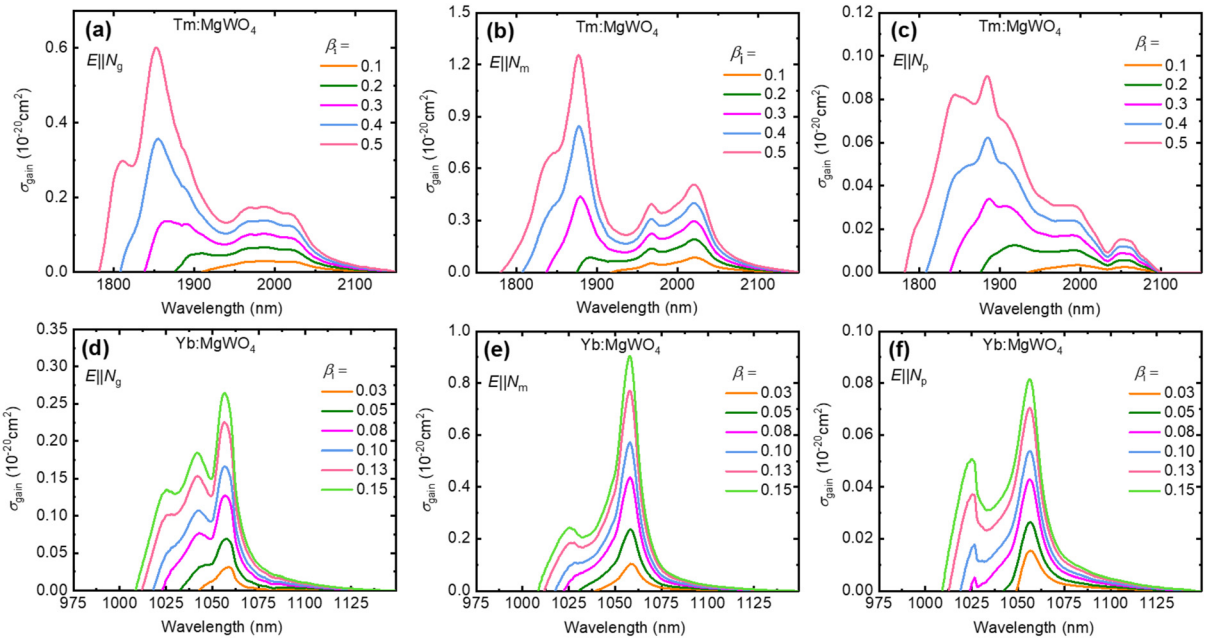

Fig. 12 Gain cross sections, σ_{gain}, for (a–c) Tm^{3+}-doped and (d–f) Yb^{3+}-doped monoclinic $MgWO_4$ for polarizations along the principal optical axes $E||N_g$ (a and d), N_m (b and e), and N_p (c and f), respectively.

cross-sections, σ_{gain}. The gain profiles for Tm^{3+} and Yb^{3+} doped $MgWO_4$ were calculated using the relation $\sigma_{gain} = \beta_i\sigma_{SE} - (1 - \beta_i)\sigma_{abs}$, where $\beta_i = N_2/N_{RE}$ represents the population inversion ratio, *i.e.* the ratio of dopant ions in the excited state, N_2, to the total ion density N_{RE}. Here, N_2 corresponds to the upper laser states $^3F_4$ for Tm^{3+} and $^2F_{5/2}$ for Yb^{3+}.

The gain spectra associated with the $^3F_4 \rightarrow {}^3H_6$ transition in Tm^{3+}:$MgWO_4$ are displayed in Fig. 12(a)–(c) for the three principal light polarizations $E||N_g$, N_m, N_p. The maximum σ_{gain} is observed for the $E||N_m$ polarization, with a local maximum at ~2020 nm at lower inversion ratios ($\beta_i < 0.3$), which suggest a linearly polarized laser output along N_m at wavelengths exceeding 2 μm. This wavelength range is accessible due to the pronounced Stark splitting of the Tm^{3+} ground-state ($^3H_6$) in $MgWO_4$, $\Delta E(^3H_6) = 633\ cm^{-1}$,[23] an important advantage over the monoclinic double tungstates such as Tm^{3+}:$KLu(WO_4)_2$ when it comes to mode-locking in the sub-100 fs regime in relation to structured water vapor air absorption below 2 μm.[21,25] No such local maximum is seen for the other strong polarization $E||N_g$. One of these two polarizations will be naturally selected for any principal cut of the laser element. All previous laser studies have been based on the strongest $E||N_m$ output polarization (sometimes designated as $E||Y$).

The polarized σ_{gain} spectra corresponding to the $^2F_{5/2} \rightarrow {}^2F_{7/2}$ transition in Yb^{3+}:$MgWO_4$ are shown in Fig. 12(d)–(f). Again, the $E||N_m$ polarization yields the highest σ_{gain} centered around 1057 nm. This is consistent with previously reported linear output polarization from Yb:$MgWO_4$ lasers. The only occasion when $E||N_g$ was utilized was in a mode-locked

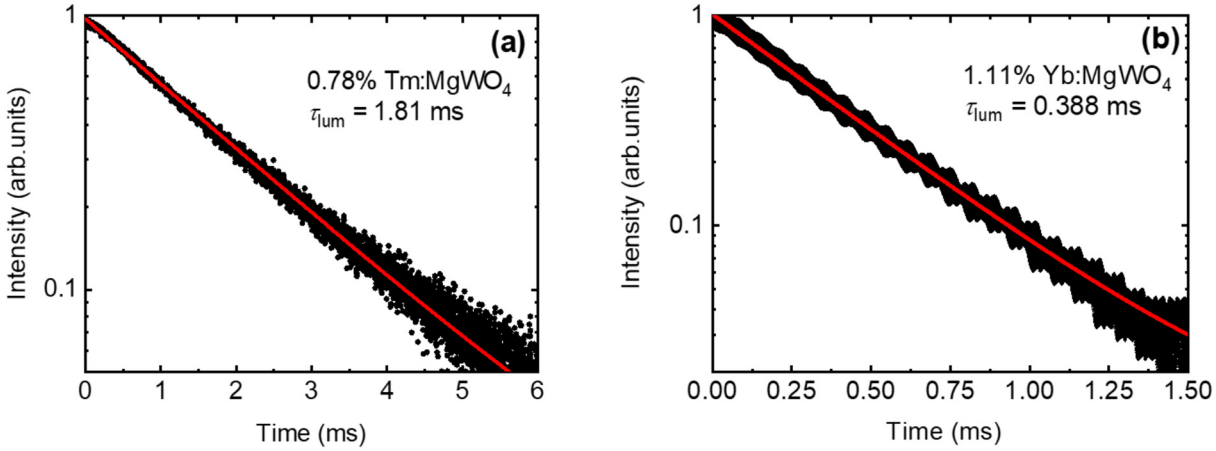

Fig. 13 Decay curves of (a) the Tm^{3+} $^3F_4$ state and (b) the Yb^{3+} $^2F_{5/2}$ state in $MgWO_4$: symbols – experimental data, solid lines – single-exponential fits.

laser,[21] just to confirm that its performance is inferior notwithstanding the superior absorption efficiency, *cf.* Fig. 11(b). Note that the weakest polarization $E||N_p$ has never been studied in a Tm or Yb lasers based on $MgWO_4$. It can be only imposed by a Brewster angle of the laser element surfaces and is potentially interesting only in Q-switched lasers to obtain higher output energies and peak powers.

Compared to previously reported σ_{gain} calculations for both Tm^{3+} and Yb^{3+} doped $MgWO_4$ crystals, our results are higher[20,22,24] or much higher and different compared to ref. 3 where the *XYZ* frame was used; note also that there shall be typographical errors in Fig. 3 of ref. 20 where these cross-sections for Yb^{3+}:$MgWO_4$ shall be actually ten times higher.

The luminescence lifetimes (τ_{lum}) of the $^3F_4$ state of Tm^{3+} and the $^2F_{5/2}$ state of Yb^{3+} in $MgWO_4$ were determined through temporal decay measurements. For Tm^{3+} ions excited at 793 nm, the luminescence decay at 1878 nm was monitored, see Fig. 13(a), revealing a lifetime of 1.81 ms. This value is comparable to the previously reported lifetime for Tm^{3+}:$MgWO_4$, τ_{lum} = 1.93 ms (ref. 24) and Tm^{3+},Li^+:$ZnWO_4$, τ_{lum} = 2.08 ms.[38] For Yb^{3+}:$MgWO_4$, the lifetime was derived by exciting Yb^{3+} at 966 nm and monitoring the luminescence at 1057 nm, see Fig. 13(b), yielding a decay constant of 388 μs. This result aligns with earlier measurements for Yb^{3+}:$MgWO_4$ (366 μs),[3] and Yb^{3+},Li^+:$ZnWO_4$ (367 μs).[39] Notably, the decay curves exhibited a single exponential pattern, consistent with the presence of a single site for both Tm^{3+} and Yb^{3+} ions in $MgWO_4$.

Conclusions

In summary, we have successfully grown monoclinic $MgWO_4$ crystals, both undoped and doped with Tm^{3+} and Yb^{3+} ions, using $K_2W_2O_7$ as a solvent for the first time. This method significantly reduced the growth time to 15 days, which is half the duration reported in previous studies for crystals of similar size. We also determined the orientation of the principal optical axes relative to the crystallographic axes and obtained polarized absorption, stimulated emission, and gain cross-section spectra for the relevant transitions of the Tm^{3+} and Yb^{3+} ions, as well as polarized Raman spectra.

Our analysis revealed that the angle between the principal optical axis N_g, corresponding to the highest refractive index, and the crystallographic axis c is only 5 ± 1°. This finding corrects a recurring error in prior studies regarding the orientation of $MgWO_4$ crystals. The partial consistency of our absorption and stimulated emission cross-section data with some of the literature further supports that previous misidentifications were likely due to incorrect crystallographic axes orientation. However, it is difficult to evaluate the impact of wrong active element orientation in previous laser experiments carried out with Tm^{3+}:$MgWO_4$ and Yb^{3+}:$MgWO_4$ crystals. They were all based on the best $E||N_m$ polarization.[3,7,18–26] The direction N_m is in fact easy to identify since in $MgWO_4$ it is perpendicular to a natural crystal surface, however, the crystal cut utilizing this polarization might be still erroneous. A wrong cut for the propagation direction might result in lower gain cross-sections even though the propagating beam in the crystal is an eigen polarization, when this happens in a principal plane containing the N_m principal optical axis.

Summarizing, the doped $MgWO_4$ crystals exhibit broad spectral bands and pronounced polarization anisotropy in their transition cross-sections, and both with Tm and Yb active ions are very promising for high-power sub-100 fs pulse generation from mode-locked lasers.

Data availability

The data supporting our findings are available from the corresponding author upon reasonable request.

Conflicts of interest

There are no conflicts to declare.

Acknowledgements

This work was financially supported by project PID2022-141499OB-100, funded by MICIU/AEI/10.13039/501100011033/ and by FEDER/UE.

References

1 J. Zhang, J. Pan, J. Yin, J. Wang, J. Pan, H. Chen and R. Mao, Structural investigation and scintillation properties of Cd1−xZnxWO4 solid solution single crystals, *CrystEngComm*, 2015, **17**, 3503–3508.

2 X. Wang, Z. Fan, H. Yu, H. Zhang and J. Wang, Characterization of $ZnWO_4$ Raman crystal, *Opt. Mater. Express*, 2017, **7**, 1732–1744.

3 L. Zhang, W. Chen, J. Lu, H. Lin, L. Li, G. Wang, G. Zhang and Z. Lin, Characterization of growth, optical properties, and laser performance of monoclinic Yb:$MgWO_4$ crystal, *Opt. Mater. Express*, 2016, **6**, 1627–1634.

4 J. Chen, L. Dong, F. Liu, H. Xua and J. Liu, Investigation of Yb:CaWO4 as a potential new self-Raman laser crystal, *CrystEngComm*, 2021, **23**, 427–435.

5 P. A. Popov, S. A. Skrobov, E. V. Zharikov, D. A. Lis, K. A. Subbotin, L. I. Ivleva, V. N. Shlegel', M. B. Kosmyna and A. N. Shekhovtsov, Investigation of the thermal conductivity of tungstate crystals, *Crystallogr. Rep.*, 2018, **63**, 111–116.

6 D. Kumar, B. P. Singh, M. Srivastava, A. Srivastava, P. Singh, A. Srivastava and S. K. Srivastava, Structural and photoluminescence properties of thermally stable Eu^{3+} activated $CaWO_4$ nanophosphor via Li^+ incorporation, *J. Lumin.*, 2018, **203**, 507–514.

7 L. Zhang, P. Loiko, J. M. Serres, E. Kifle, H. Lin, G. Zhang, E. Vilejshikova, E. Dunina, A. Kornienko, L. Fomicheva, U. Griebner, V. Petrov, Z. Lin, W. Chen, K. Subbotin, M. Aguiló, F. Díaz and X. Mateos, Growth, spectroscopy and first laser operation of monoclinic Ho^{3+}:$MgWO_4$ crystal, *J. Lumin.*, 2019, **213**, 316–325.

8 E. Cavalli, A. Belletti and M. G. Brik, Optical spectra and energy levels of the Cr^{3+} ions in MWO_4 (M=Mg, Zn, Cd) and $MgMoO_4$ crystals, *J. Phys. Chem. Solids*, 2008, **69**, 29–34.

9 P. F. Schofield, K. S. Knight and G. Cressey, Neutron powder diffraction study of the scintillator material $ZnWO_4$, *J. Mater. Sci.*, 1996, **31**, 2873–2877.

10 V. B. Kravchenko, Crystal structure of the monoclinic form of magnesium tungstate $MgWO_4$, *J. Struct. Chem.*, 1969, **10**, 139–140.

11 L. Zhang, Y. Huang, S. Sun, F. Yuan, Z. Lin and G. Wang, Thermal and spectral characterization of Cr^{3+}:$MgWO_4$—a promising tunable laser material, *J. Lumin.*, 2016, **169**, 161–164.

12 E. N. Sota, F. Che Ros and J. Hassan, Synthesis and characterisation of AWO_4 (A = Mg, Zn) tungstate ceramics, *J. Phys.: Conf. Ser.*, 2018, **1083**, 012002.

13 S. Wannapop, T. Thongtem and S. Thongtem, Photoemission and energy gap of $MgWO_4$ particles connecting as nanofibers synthesized by electrospinning–calcination combinations, *Appl. Surf. Sci.*, 2012, **258**, 4971–4976.

14 J. Meng, T. Chen, X. Wei, J. Li and Z. Zhang, Template-free hydrothermal synthesis of $MgWO_4$ nanoplates and their application as photocatalysts, *RSC Adv.*, 2019, **9**, 2567–2571.

15 F. A. Danevich, D. M. Chernyak, A. M. Dubovik, B. V. Grinyov, S. Henry, H. Kraus, V. M. Kudovbenko, V. B. Mikhailik, L. L. Nagornaya, R. B. Podviyanuk, O. G. Polischuk, I. A. Tupitsyna and Y. Y. Vostretsov, $MgWO_4$–A new crystal scintillator, *Nucl. Instrum. Methods Phys. Res., Sect. A*, 2009, **608**, 107–115.

16 V. B. Mikhailik, H. Kraus, V. Kapustyanyk, M. Panasyuk, Y. Prots, V. Tsybulskyi and L. Vasylechko, Structure, luminescence and scintillation properties of the $MgWO_4$–$MgMoO_4$ system, *J. Phys.: Condens. Matter*, 2008, **20**, 365219.

17 L. Li, Y. Yu, G. Wang, L. Zhang and Z. Lin, Crystal growth, spectral properties and crystal field analysis of Cr^{3+}:$MgWO_4$, *CrystEngComm*, 2013, **15**, 6083–6089.

18 J. Lu, H. Lin, G. Zhang, B. Li, L. Zhang, Z. Lin, Y.-F. Chen, V. Petrov and W. Chen, Direct generation of an optical vortex beam from a diode-pumped Yb:$MgWO_4$ laser, *Laser Phys. Lett.*, 2017, **14**, 085807.

19 H. Lin, G. Zhang, L. Zhang, Z. Lin, F. Pirzio, A. Agnesi, V. Petrov and W. Chen, Continuous-wave and SESAM mode-locked femtosecond operation of a Yb:$MgWO_4$ laser, *Opt. Express*, 2017, **25**, 11827–11832.

20 P. Loiko, M. Chen, J. M. Serres, M. Aguiló, F. Díaz, H. Lin, G. Zhang, L. Zhang, Z. Lin, P. Camy, S.-B. Dai, Z. Chen, Y. Zhao, L. Wang, W. Chen, U. Griebner, V. Petrov and X. Mateos, Spectroscopy and high-power laser operation of a monoclinic Yb^{3+}:$MgWO_4$ crystal, *Opt. Lett.*, 2020, **45**, 1770–1773.

21 Y. Wang, W. Chen, M. Mero, L. Zhang, H. Lin, Z. Lin, G. Zhang, F. Rotermund, Y. J. Cho, P. Loiko, X. Mateos, U. Griebner and V. Petrov, Sub-100 fs Tm:$MgWO_4$ laser at 2017 nm mode locked by a graphene saturable absorber, *Opt. Lett.*, 2017, **42**, 3076–3079.

22 P. Loiko, J. M. Serres, X. Mateos, M. Aguilo, F. Diaz, L. Zhang, Z. Lin, H. Lin, G. Zhang, K. Yumashev, V. Petrov, U. Griebner, Y. Wang, S. Y. Choi, F. Rotermund and W. Chen, Monoclinic Tm^{3+}:$MgWO_4$: a promising crystal for continuous-wave and passively Q-switched lasers at ~2 μm, *Opt. Lett.*, 2017, **42**, 1177–1180.

23 P. Loiko, Y. Wang, J. M. Serres, X. Mateos, M. Aguiló, F. Díaz, L. Zhang, Z. Lin, H. Lin, G. Zhang, E. Vilejshikova, E. Dunina, A. Kornienko, L. Fomicheva, V. Petrov, U. Griebner and W. Chen, Monoclinic Tm:$MgWO_4$ crystal: Crystal-field analysis, tunable and vibronic laser demonstration, *J. Alloys Compd.*, 2018, **763**, 581–591.

24 L. Zhang, H. Lin, G. Zhang, X. Mateos, J. M. Serres, M. Aguiló, F. Díaz, U. Griebner, V. Petrov, Y. Wang, P. Loiko, E. Vilejshikova, K. Yumashev, Z. Lin and W. Chen, Crystal growth, optical spectroscopy and laser action of Tm^{3+}-doped monoclinic magnesium tungstate, *Opt. Express*, 2017, **25**, 3682–3693.

25 L. Wang, W. Chen, Y. Zhao, Y. Wang, Z. Pan, H. Lin, G. Zhang, L. Zhang, Z. Lin, J. E. Bae, T. G. Park, F. Rotermund, P. Loiko, X. Mateos, M. Mero, U. Griebner and V. Petrov, Single-walled carbon-nanotube saturable absorber assisted Kerr-lens mode-locked Tm:$MgWO_4$ laser, *Opt. Lett.*, 2020, **45**, 6142–6145.

26 E. Kifle, P. Loiko, J. R. Vazquez De Aldana, C. Romero, V. Llamas, J. M. Serres, M. Aguilo, F. Diaz, L. Zhang, Z. Lin, H. Lin, G. Zhang, V. Zakharov, A. Veniaminov, V. Petrov, U. Griebner, X. Mateos and W. Chen, Low-loss fs-laser-written surface waveguide lasers at >2 μm in monoclinic Tm^{3+}:$MgWO_4$, *Opt. Lett.*, 2020, **45**, 4060–4063.

27 R. D. Shannon and C. T. Prewitt, Revised values of effective ionic radii, *Acta Crystallogr., Sect. B*, 1970, **26**, 1046–1048.

28 A. Lupei, V. Lupei, C. Gheorghe, L. Gheorghe and A. Achim, Multicenter structure of the optical spectra and the charge-compensation mechanisms in Nd: $SrWO_4$ laser crystals, *J. Appl. Phys.*, 2008, **104**, 083102.

29 W. Kolbe, K. Petermann and G. Huber, Broadband emission and laser action of Cr^{3+} doped zinc tungstate at 1 μm wavelength, *IEEE J. Quantum Electron.*, 1985, **21**, 1596–1599.

30 L. Zhang, L. Basyrova, P. Loiko, P. Camy, Z. Lin, G. Zhang, S. Slimi, R. M. Solé, X. Mateos, M. Aguiló, F. Díaz, E. Dunina, A. Kornienko, U. Griebner, V. Petrov, L. Wang and W. Chen, Growth, structure, and polarized spectroscopy of monoclinic Er^{3+}:$MgWO_4$ crystal, *Opt. Mater. Express*, 2022, **12**, 2028–2040.

31 A. Le Bail, Whole powder pattern decomposition methods and applications: A retrospection, *Powder Diffr.*, 2005, **20**, 316–326.

32 N. J. Dunning and H. D. Megaw, The crystal structure of magnesium tungstate, *Trans. Faraday Soc.*, 1946, **42**, 705–709.

33 J. Ruiz-Fuertes, D. Errandonea, S. López-Moreno, J. González, O. Gomis, R. Vilaplana, F. J. Manjón, A. Muñoz, P. Rodríguez-Hernández, A. Friedrich, I. A. Tupitsyna and L. L. Nagornaya, High-pressure Raman spectroscopy and lattice-dynamics calculations on scintillating $MgWO_4$: Comparison with isomorphic compounds, *Phys. Rev. B: Condens. Matter Mater. Phys.*, 2011, **83**, 214112.

34 V. Petrov, M. C. Pujol, X. Mateos, Ò. Silvestre, S. Rivier, M. Aguiló, R. M. Solé, J. Liu, U. Griebner and F. Díaz, Growth and properties of $KLu(WO_4)_2$, and novel ytterbium and thulium lasers based on this monoclinic crystalline host, *Laser Photonics Rev.*, 2007, **1**, 179–212.

35 G. Z. Elabedine, K. Subbotin, P. Loiko, Y. Zimina, S. Pavlov, A. Titov, P. Camy, A. Braud, R. M. Solé, M. Aguiló, F. Díaz, W. Chen, X. Mateos and V. Petrov, Monoclinic Yb^{3+},Li^{+}:$ZnWO_4$ – efficient broadly emitting laser material, *Proc. SPIE*, 2024, **12864**, 128640K.

36 B. F. Aull and H. P. Jenssen, Vibronic interactions in Nd:YAG resulting in nonreciprocity of absorption and stimulated emission cross sections, *IEEE J. Quantum Electron.*, 1982, **18**, 925–930.

37 S. A. Payne, L. L. Chase, L. K. Smith, W. L. Kway and W. F. Wyers, Infrared cross-section measurements for crystals doped with Er^{3+}, Tm^{3+}, and Ho^{3+}, *IEEE J. Quantum Electron.*, 1992, **28**, 2619–2630.

38 G. Z. Elabedine, K. Subbotin, P. Loiko, Z. Pan, Y. Zimina, K. Kuleshova, A. Titov, A. Nady, P. Camy, A. Braud, R. M. Solé, M. Aguiló, F. Díaz, W. Chen, W. Chen, X. Mateos, X. Mateos and V. Petrov, Monoclinic Tm^{3+}:$ZnWO_4$: Novel 2 μm laser crystal, *Advanced Solid State Lasers Conference*, Tacoma (WA), USA, Oct 8, 2023, vol. 12, OPTICA Online Technical Digest, paper AW1A.5.

39 A. Volokitina, S. P. David, P. Loiko, K. Subbotin, A. Titov, D. Lis, R. M. Solé, V. Jambunathan, A. Lucianetti, T. Mocek, P. Camy, W. Chen, U. Griebner, V. Petrov, M. Aguiló, F. Díaz and X. Mateos, Monoclinic zinc monotungstate Yb^{3+},Li^{+}:$ZnWO_4$: Part II. Polarized spectroscopy and laser operation, *J. Lumin.*, 2021, **231**, 117811.